Springer

KSME

Journal of Mechanical Science and Technology 29 (7) (2015) 2847~2856
www.springerlink.com/content/1738-494x(Print)/1976-3824(Online)
DOI 10.1007/s12206-015-0613-0

Effect of the indentation process on fatigue life of drilled specimens †

Giuseppe Marannano[1,*], Antonino Pasta[1], Francesco Parrinello[2] and Antonio Giallanza[1]

[1]*Dept. of Chemical, Management, Computer Science and Mechanical Engineering, University of Palermo, Palermo, Italy*
[2]*DICAM, University of Palermo, Palermo, Italy*

(Manuscript Received December 1, 2014; Revised March 4, 2015; Accepted March 11, 2015)

Abstract

Design and manufacture of mechanical elements are strongly influenced by the evaluation of the residual stresses due to their effects on the material strength. This paper presents numerical and experimental results performed on AW 6082-T6 aluminum alloy drilled specimens when the hole is created after a bilateral indentation process. The plastic deformation induced by the indenters creates a compressive residual stress field around the hole, which persists after the drilling operation. Several numerical analysis have been carried out in ANSYS APDL explicit solver for different indentation depths and hole diameters in order to evaluate the compressive circumferential stresses, optimal process parameters and relevant geometric features. Fatigue tests are performed in order to determine the cycles to failure and the corresponding Wöhler diagram.

Keywords: Indentation process; Cold working; FE analysis; Residual stress; Fatigue

1. Introduction

The study on the fatigue behavior of drilled structures shows that, due to the presence of high stress concentration, the coalescence of micro-cracks often arise in the area around the hole. Several literature studies are focused on the research of methods that delay the onset and propagation of fatigue cracks. Among the most commonly methods used in industrial processes, plastic deformation techniques increase the fatigue life of mechanical components because they generate beneficial compressive residual stress fields.

Yoon et al. [1] investigate the shot-peening effects on the fatigue life behavior of bearing steel. Results of a rotary bending fatigue test show that shot-peening suppressed not only much of the surface-originated fracture but also the scattering error of the probabilistic stress-life data, and improve the fatigue life by about six times through the load levels of the cyclic tests. Im et al. [2] use laser peening (LP) in order to induce high-magnitude compressive residual stresses in a small region of a mechanical component. The compressive residual stresses cause plastic deformation that is resistant to fatigue fracture.

In addition to the mentioned techniques, the cold expansion process is a simple life enhancement procedure that strengthens metallic components by retarding crack growth around the hole [3]. The most common methods of cold working are accomplished by using a conical mandrel or an over-sized ball. The force plastically expands the hole beyond the material yield point, producing a residual compressive stress zone around the hole itself.

The literature presents several studies in order to evaluate the residual stress field around the expanded hole. Hsu & Forman [4] estimate the residual stress state in a plane stress condition by considering an infinite elastic-plastic plate having a hole submitted to internal pressure. Rich and Impellizzeri [5] present an approximate solution for residual stress distribution around the cold expanded holes based on elastic-perfectly plastic behavior of materials. D'Acquisto et al. [6] estimate the location of the elastic-plastic boundary by means of experimental measurements of the out-of-plane displacement surrounding cold-expanded holes on a 6082-T6 aluminum alloy specimens. Lai et al. [7] investigate the residual stress distribution around cold worked holes on ballised specimens. In particular, the effects of interference levels and specimen size on residual stresses are studied. The study confirms that the ballising method introduces large compressive residual stresses onto the surface of a cold worked hole; the technique, therefore, has the potential to give significant enhancement in the fatigue performance of the hole.

More recently, some authors use the finite element method in order to study the residual stresses distribution around the cold expanded hole. Poussard et al. [8] model the radial expansion process, introducing uniform expansion through the

*Corresponding author. Tel.: +39 91 238 97270, Fax.: +39 91 7025040
E-mail address: giuseppe.marannano@unipa.it
† Recommended by Associate Editor Nam-Su Huh
© KSME & Springer 2015

plate thickness. Expansion and its degree influence are studied using 2D finite element analysis. Chakherlou at al. [9] perform 3D numerical analyses using conical mandrels. Ismonov et al. [10], whereas, simulate the mandrels reproducing the real geometry. The comparison of these studies revealed that the mandrel geometry has a significant effect on the residual stress field. In Aid et al. [11], finite element models have been established to bind the crack growth from an expanded hole. Stress intensity factors are determined and used to evaluate the fatigue life. Residual stress field is evaluated using a nonlinear analysis and superposed with the applied stresses field in order to estimate fatigue crack growth. Seifi et al. [12] show experimental and numerical results for two different aluminum alloys and various holes distances. The maximum expansion level used is about 4%. Effects of some parameters such as hole diameters and their distances, thickness of plate and level of cold expansion on residual stress distribution are studied. Based on experimental tests and numerical simulations, Kim et al. [13] show the optimal results in case of adjacent holes. Their show that if the distance between holes is more than four times of the diameter of the hole, the residual stress around holes is not influenced by adjacent holes. Chakherlou et al. [14] studied, numerically and experimentally, the effects of cold expanding on the Al-2024-T3 connections. They show that the specimens with cold expanded holes have larger fatigue life. Baburamani et al. [15] present the results involving constant amplitude fatigue loading of open hole coupons with and without cracks. The fatigue life improvement achieved by the use of hole cold expansion technology are presented. The cold expansion process has, however, the big drawback of generating non-uniform stress distribution between mandrel entry side and mandrel exit side. In fact, the split sleeve, used to preserve the hole during the expansion process, generates an asymmetric distribution of residual radial stresses. It also presents a substantial limitation related to the maximum expansion level that can be applied (about 4-4.5% on aluminum alloys). In fact, over such a value, the edge of the hole can be damaged causing the coalescence of micro-cracks. In this study, the examined technique overcomes the above-mentioned limitations.

This paper presents numerical and experimental analysis performed on AW 6082-T6 aluminum alloy drilled specimens when the hole is created after a bilateral indentation process [16-18]. In Ref. [19], the instrumented indentation is used to measure a variety of mechanical properties (Hardness, Young's modulus, yield strength, work-hardening exponent, creep stress exponent, fracture toughness) and to estimate residual stresses. In this paper, instead, the indentation process is only used in order to create a compressive residual stress field around the hole, which persists after the drilling operation. Moreover, the technique preserves from localized damages because the hole is realized after the indentation step. Indentation process involves plasticity and induces a plastic zone, and the associated stress solution is a classic contact mechanics problem. To solve this problem, there are mainly analytical and computational approaches. Because of the complexity of the problem, most of the analytical approaches can only be solved numerically. Although the stress fields around purely elastic indentations can be described in closed form for indenters with various geometries the indentation process is generally elasto-plastic and forms a contact-induced plastic deformation zone, making the analysis very complex. Feng et al. [20, 21] propose an analytical model in order to estimate the stress field around an elastoplastic indentation/contact. Analytical results are in good agreement with the finite element analysis. In Ref. [22], Yang et al. study the effect of the indenter size on the indentation of aluminum. In particular, the paper discuss the evolution of dislocations in indentation and the effect of the size of indenter on the relation between the indentation stress and strain.

In the present paper, several numerical analysis, conducted in ANSYS APDL explicit solver environment, allow to determine the trend of the circumferential residual stress by varying indentation depth and hole diameter. The numerical model has been validated by comparison between the residual surface profile obtained by finite element simulations, after indentation step, and the corresponding one obtained by means of Comet 5^{TM} 3D Steinbichler laser scanner [6].

Numerical results are compared with experimental tests conducted on AW 6082-T6 aluminum alloy specimens with a thickness of 5 mm. Several fatigue tests were conducted to determine the cycles to failure and the corresponding Wöhler diagram. Experimental results were compared with those obtained from only drilled specimens.

2. Indentation and drilling process

Similarly to cold expansion process, the indentation process determine the onset of residual stresses in a limited area of the structure. The process is performed by using a pairs of specialized tools called indenters or punches (Fig. 1) that act simultaneously on both sides of the plate until a specified depth (Fig. 1(a)), on two points of the opposing faces where the hole will be performed.

The shape of the indenters influences the residual stress zone surrounding the hole and through the thickness of the plate. In the present paper, spherical punches are considered.

When the indenters is removed, spherical cavity appears evident on the two surfaces of the plate, as effect of the induced permanent deformation. The spherical cavities are typically smaller than the final hole and they are removed when the hole is realized (Fig. 1(b)).

The process is relatively simple to be performed and does not require particularly complex tools and methods. For the execution of the process, spherical elements manufactured from hardened steel have been used and positioned on a C40 steel support, hardened at high temperature (Fig. 1(c)). The indentation phase produces effects only on a restricted zone (Action field of the indenters) where deformations exceed the yield point producing plastic phenomena. In the indenters

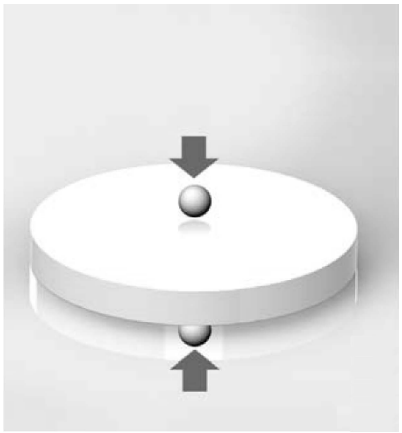

(a)

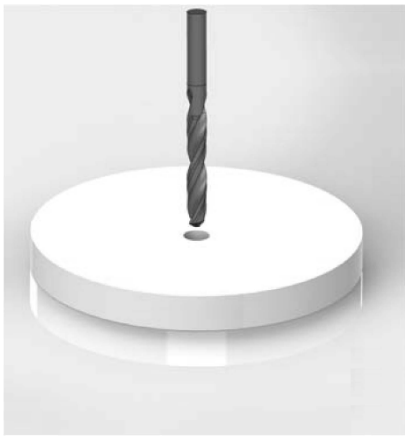

(b)

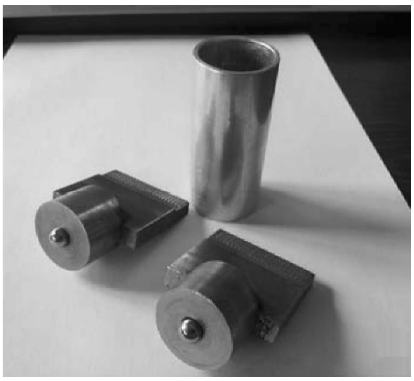

(c)

Fig. 1. (a) Indentation phase; (b) drilling phase; (c) spherical indenters used for indentation process.

removal phase, the elastic stresses field tends to restore the original configuration: this is not very feasible due to the presence of permanent deformations generated in the neighborhood of the punches themselves [23-27].

Finally, the drilling operation modify the geometry domain and the residual stresses field adapts to the new geometry: On the surface of the hole, the radial component reduces to zero and the circumferential one keeps a compressive stress state.

Table 1. Constitutive parameter of AW 6082-T6 aluminum alloy.

Density [Kg/mm^3]	$2.7 \cdot 10^{-6}$
Young modulus [MPa]	69000
Poisson modulus	0.33
Proof stress 0.2% [MPa]	260
Tensile strength (MPa)	310
Shear strength (MPa)	210
Elongation A5 (%)	11
Hardness vickers (HV)	100
Tangent modulus [MPa]	20
Hardening parameter	0.5

3. Numerical model

Several numerical analyses have been conducted in ANSYS by means of routines written in APDL environment with explicit solver, a general-purpose transient dynamic finite element program capable of simulating complex problems including non-linear material behavior such as cold working [28]. The procedure involves the parametric definition of both model and process phases and it provides an accurate assessment of strength improvement of the drilled plates.

Similarly to the real process, the problem is generally analyzed by following two distinct phases, indentation and drilling phase. In the first operation, indenters of defined geometry penetrate and move away from the plate according to appropriate time function. In the second phase, elements corresponding to the volume to be drilled are removed from the indented plate. It is necessary to wait for residual stresses redistribution. Each analysis is divided into two different subroutines, respectively for indentation and drilling phase. The parametric model is discretized by means of eight-nodes elements (SOLID164), used for the three-dimensional modeling of solid structures. The material is constitutively modeled as elasto-plastic with kinematic hardening behavior. The relevant parameters of AW 6082-T6 aluminum alloy are collected in Table 1.

Indenters are defined as rigid elements in order to reduce the analysis time. The Fig. 2(a) shows a detail of discretization, with increased spacing ratio in the neighborhood of the hole.

The FE model is defined by two concentric cylindrical volumes: the first one representing the drilling zone (Diameter d) and the second one (Outer diameter $D_e = 6d$) as the representative portion of the plate where the residual stresses are evaluated. The thickness of the model is 5 mm.

Node-to-surface (NTS) contact elements are used to define the contact between the plate and indenters. The loading phase for the punching operation is defined in terms of imposed displacement of the indenters and the relevant displacement *vs* time curves are represented in Fig. 2(b). The time steps are $\Delta t = 0.1s$. The second numerical analysis, which reproduces the effects of drilling operation, starts from the last equilibrium condition reached by the first procedure. Therefore, the

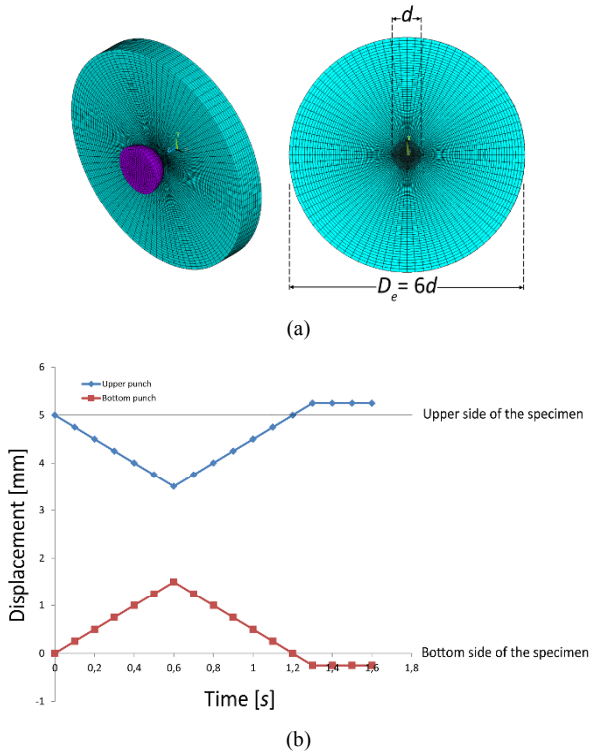

Fig. 2. (a) Detail of FE model discretization; (b) displacement *vs* time curves of the two indenters.

finite elements discretizing the drilling volume have to be selected and removed and the numerical analysis is finally performed in order to numerically evaluate the relevant stress equilibrium state. Such numerical analysis is performed for only eight time steps (Total analysis time equal to $t = 0.8\ s$) in order to wait that the stress fluctuations amplitude in the plate become negligible. Once the analysis is completed, it is possible to plot nodal stresses and strains distribution as a function of time, the trend of the kinematic flow of the material and the residual stress through the thickness of the model.

4. Validation of numerical model

The numerical model is experimentally validated by means of optical acquisition of the residual profile (Fig. 3(a)). Moreover, the plasticity effects on the residual stresses are determined by means of strain gauge measurements. In detail, in the first case, the numerical model results are compared to the experimental ones in terms of displacement of the residual deformed configuration. On the area surrounding the hole, the indented volume overflows through the undeformed surface and induces a local plastic zone (Pile-up) [29] as a consequence of an high state of deformation and of a differential flow of material (Fig. 3(b)).

Experimental acquisition is performed by laser scanner 3D Comet5 Steinbichler™. The accuracy of the measured out-of-plane displacements is 1μm, in a direction parallel to the line-of-sight of the Comet scanner. The lateral resolution (Point-to-

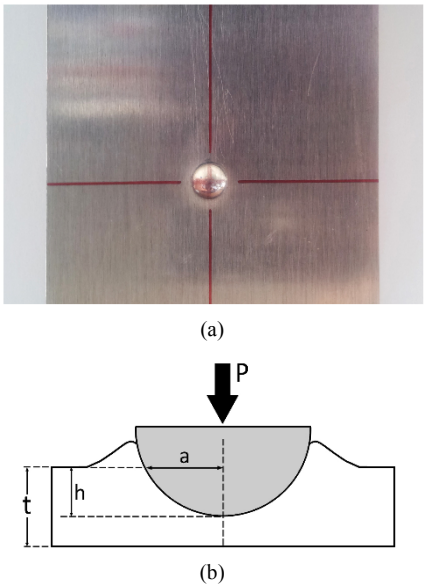

Fig. 3. (a) Dimple shape on the specimen after indentation phase; (b) schematic view of the pile-up.

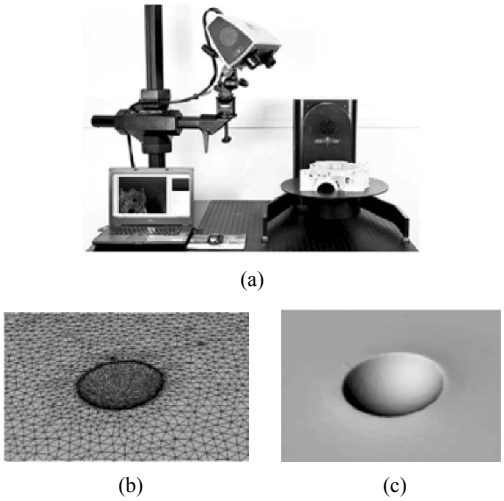

Fig. 4. (a) Scanner comet5 3D Steinbichler; (b) detail of the discretization provided by the software acquisition; (c) rendering of the dimple generated on the specimen.

point distance) is 50 μm. The highest resolution of the method is obtained when the cloud of points is focused in the smallest volume of observation (100 × 100 × 100 mm) [6]. Fig. 4(a) shows the overall layout of the acquisition system.

The laser scanning provides, as a direct result of the detection, a set of three-dimensional coordinates in a local system correlated with the instrument. The coordinates define a cloud of points of the outer surface of the scanned object. The points cloud has been exported to an STL file and points coordinates are obtained after cleaning and optimization procedures.

Fig. 4(b) shows, in particular, the mesh obtained by the acquisition software and the final render of the residual profile (Fig. 4(c)). Fig. 5 compares the transversal profiles of the in-

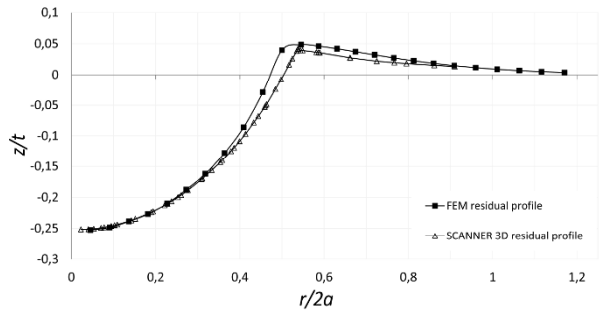

Fig. 5. Comparison between numerical and experimental residual profile.

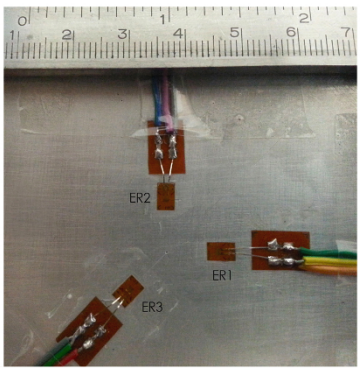

(a)

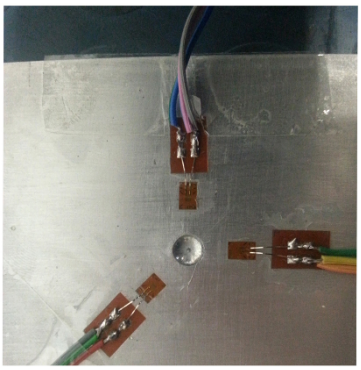

(b)

Fig. 6. Strain gauges installed around the indented area: (a) before indentation process; (b) after indentation process.

dentation zone in the residual deformed configuration obtained, respectively, through the optical acquisition and FE analysis ($h/t = 0.25$). In particular, the Fig. 5 shows the ratio of z/t (Out-of-plane displacement / specimen thickness) *vs* the dimensionless parameter $r/2a$, where r is the radial distance from the hole axis and a is the radius of the spherical cavity. The analysis is carried out considering the dimensionless ratio $h/t = 0.25$. The graph shows that the radius of the spherical cavity, evaluated numerically, differs less than 6% with respect to the one obtained experimentally. Finally, it can be observed that the out-of-the-plane displacement between experimental and numerical trends is negligible when the radial coordinate is greater than the diameter of the spherical cavity

(a)

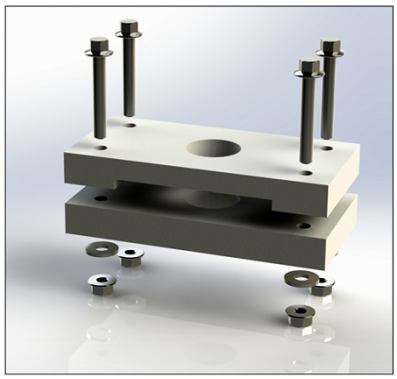

(b)

Fig. 7. (a) Indentation phase on MTS machine; (b) rendering of the prismatic jig used in the indentation step.

($r/2a \geq 0.9$). In the paper, the plasticity effects on the residual stresses are determined by means of strain gauge measurements. According to Fig. 6(a), radial strains are measured by three electrical strain gauges ER1, ER2 and ER3. The strain gauges have an active grid length equal to 0.6mm and resistance of 120 Ω. In order to obtain a redundant measurement, three independent components of plane strain are simultaneously recorded during the loading phase. The strain gauges are attached on the surface of the specimen with different angles: 0° (ER1), 90° (ER2), 225° (ER3).

The strain gauges are positioned at a distance d_0 equal to 9 mm ($d_0 = 1.55d$) from the center of the dimple, such as shown in Fig. 6(b).

During the loading phase, conducted on a MTS 810 universal testing machine, the specimen is simultaneously indented on both side of the surface (see Fig. 7(a)). The crosshead speed is set to 1mm/min. In order to support the specimen in a horizontal position during the indentation process, a prismatic jig has been properly realized (Fig. 7(b)).

Fig. 8 shows the radial strains as a function of the loading and unloading time. As can be observed from the figure, the two phases are separated by a time interval of 30*s* during which the indenters are maintained at the position of maximum depth. Residual experimental strains are compared with those obtained from finite element analysis.

Fig. 9 shows a detail of the model used in the numerical simulations. Fig. 9(a) shows a detail of the volumetric subdivision surrounding the indented area. Fig. 9(b) shows the level

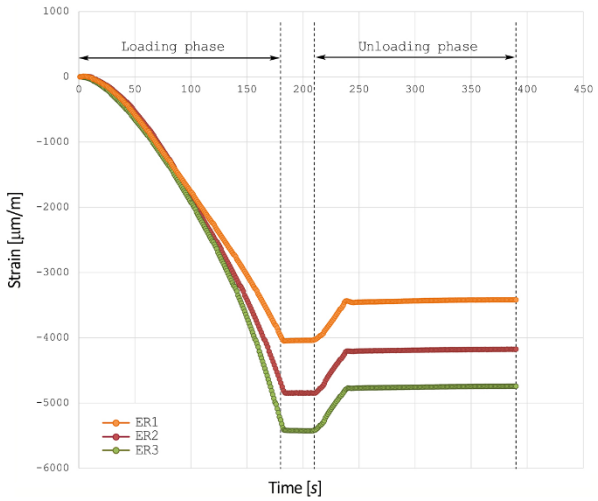

Fig. 8. Experimental trend of the radial strains measured by the three strain gauges.

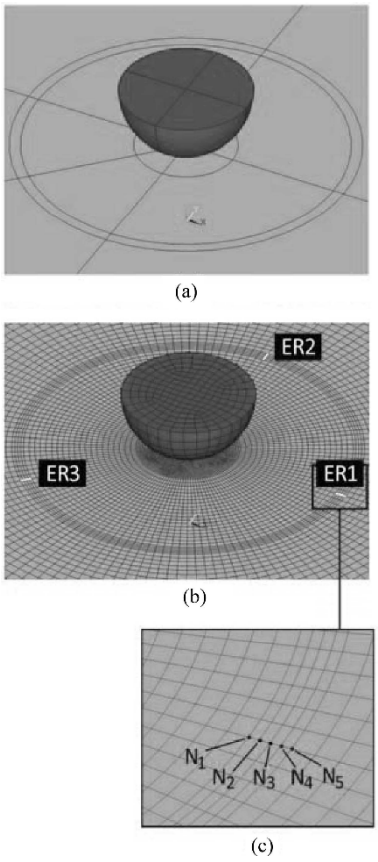

Fig. 9. (a) Volumetric subdivision surrounding the indented area; (b) detail of the discretization; (c) node numbering used for the strain gauge ER1.

of detail of the discretization and the mesh refinement around the area in which the radial strains are evaluated. As shown in Fig. 9(c), five nodes are positioned on the lines corresponding to the three strain gauges. Such nodes are marked with N_i ($1 \leq i \leq 5$). In agreement with the strain gauges positioning

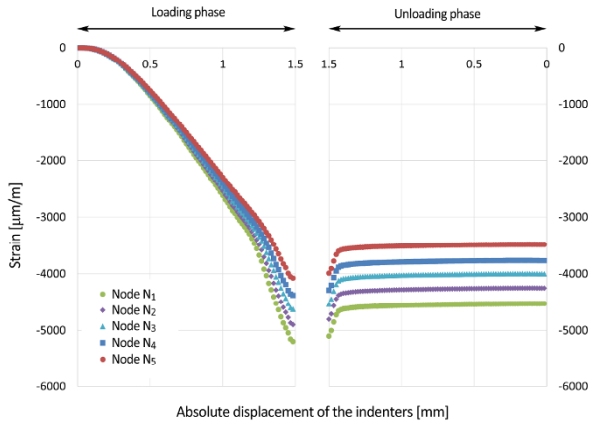

Fig. 10. Numerical trend of radial strains measured in the nodes N_1, N_2, N_3, N_4, and N5 during the loading and unloading phase.

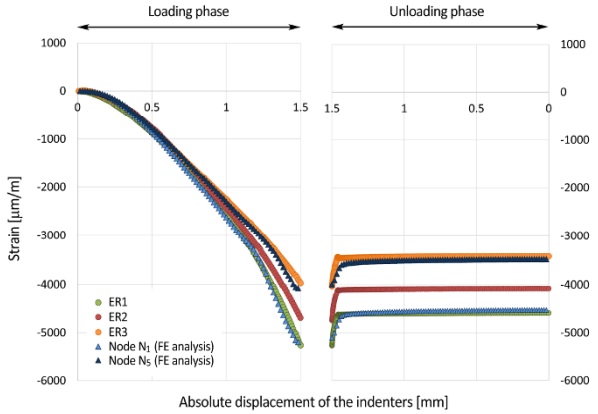

Fig. 11. Comparison between experimental and numerical radial deformation during loading and unloading phase.

shown in Fig. 6, the node N_3 is positioned at a distance of 9mm from the indenter axis. The relative distance between the nodes N_1 and N_5, measured in the radial direction, is equal to the grid length of the strain gauge (l_0 = 0.6 mm). Fig. 10 shows the trend of the radial strains as a function of the absolute displacement of the indenters, respectively, for loading and unloading phase and related to the nodes corresponding to the position of the strain gauge ER1. FE analysis show that strains value of the nodes corresponding to the strain gauge ER1 and those corresponding to the strain gauges ER2 and ER3 differ by less than 1%. Therefore, trends related to the strain gauges ER1 and ER2 are omitted in Fig. 10.

Fig. 11 shows the comparison between experimental and numerical radial deformation during loading and unloading phase. In particular, Fig. 11 shows the experimental measurement of strain compared with the trends obtained from numerical simulation measured in the external nodes N_1 and N_5. The experimental results are in good agreement with the numerical data. The strain gauges ER1 and ER3 provide residual strain values that differ by an amount equal to 26%. This difference, as demonstrated by numerical analysis, could be at-

Table 2. Parameters of indenter and indentation depth used in the numerical analysis.

Indenter radius [mm]	4.73	4.01	3.57	3.29
Indentation depth [mm]	1	1.25	1.5	1.75
Hole diameter [mm]	5.8	5.8	5.8	5.8
	6.8	6.8	6.8	6.8
	7.8	7.8	7.8	7.8

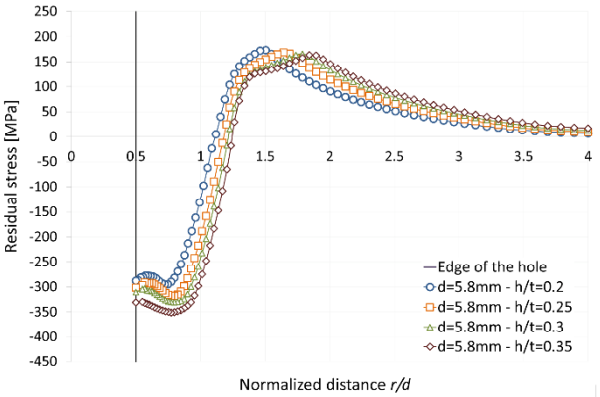

Fig. 12. Residual stress distributions *vs* the dimensionless parameter *r/d* for different values of indentation depth.

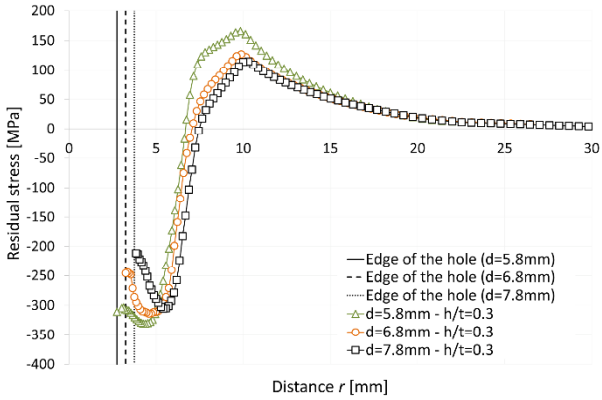

Fig. 13. Residual stress distributions *vs* the distance *r* from the hole axis for different values of the final hole diameter.

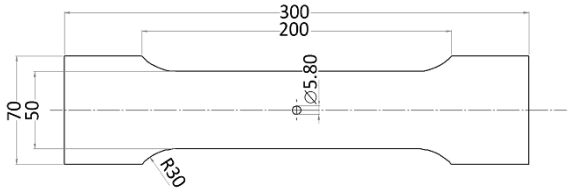

Fig. 14. Geometric characteristics of the specimens.

tributed to an inaccuracy in the position of the strain gauges, about a few tenths of a millimeter. In fact, as shown by the numerical simulation, the residual strain values measured in the external nodes N_1 e N_5 differ by an amount equal to 23%.

In conclusion, considering the small differences between experimental and numerical analysis, the residual stress field obtained by the numerical simulation can reasonably be considered reliable.

5. Numerical analysis results

Several numerical analyses have been performed with different values of indentation depth, spherical indenters radius and final hole diameter. The adopted values are reported in Table 2. In order to obtain comparable results, all the numerical simulation have been performed assuming a constant value of the radius of the spherical cavity equal to a = 2.9 mm (see Fig. 3(b), 5). Therefore, a specific indentation depth has been assumed for each spherical indenter of different radius (see Table 2).

Fig. 12 shows the circumferential residual stress distributions at the centerline of the specimen in function of the dimensionless parameter *r/d*, for a final hole diameter equal to d = 5.8 mm and different values of indentation depth. The graph of Fig. 13 shows the circumferential residual stress vs the distance r from the hole axis for a constant value of indentation depth (h/t = 0.3) and different values of the final hole diameter.

As a shown in Fig. 12, the compressive residual stress surrounding the hole increases with the depth of indentation. For indentation depth close to or greater than the value of h = 1.75 mm (h/t = 0.35), the numerical analysis provides residual stress values on the edge of the hole close to the ultimate stress of the aluminum alloy. For this reason, indentation depth values equal to or higher than h = 1.75 mm will not be taken into account in the experimental tests.

Optimal results (in terms of circumferential residual stress values on the edge of the hole) have been obtained with indentation depth of h = 1.5 mm (60% of the thickness of the plate) and final diameter of the hole equal to d = 5.8 mm, equal to the value of the spherical cavity diameter. In fact, as shown in Fig. 13, the residual stresses on the edge of the hole decreases when the final diameter increases.

6. Experimental tests

Experimental tests were conducted on a MTS 810 universal testing machine with a load cell of 100 kN. Fig. 14 shows the geometric characteristics of the specimens.

Several static and dynamic tests were conducted with varying indentation depth. Tables 3 and 4 show the total number of specimens used for static and dynamic tests.

Fig. 15 shows the experimental setup of the specimen placed on the testing machine. Static tests are performed in displacement control mode with crosshead speed of 1 mm/min. Table 5 shows the results obtained for the static tests.

Static tests results show that the indentation technique does not provide significant increases to the value of the ultimate failure load. Specimens subjected to indentation process (Type C specimen) show an increment of average ultimate load of

Table 3. Static tests.

	Only drilled specimens	Specimens subjected to indentation process	
Specimen type	A	B	C
Indenter radius [mm]	-	4.01	3.57
Indentation depth [mm]	-	1.25	1.5
Hole diameter [mm]	5.8		
Number of specimens	5	5	5

Table 4. Dynamic tests.

		Percentage of the ultimate static load			
		40%	50%	60%	70%
Specimen type	Indentation depth [mm]	Number of specimens			
A	-	3	3	3	3
B	1.25	3	4	4	3
C	1.5	4	4	4	3

Table 5. Static tests results.

Specimen type	A	B	C
Average ultimate load [kN]	70.03	71.23	72.12

Fig. 15. Specimen placed on the material testing machine.

about 2.9% compared to the only drilled specimens. Fatigue tests are performed in load control mode. The maximum applied load is imposed between 40% and 70% of the ultimate static load at a frequency of 10Hz. R-ratios (Ratio of minimum/maximum load) is equal to 0.1.

Fig. 16 shows the Wöhler diagrams for all the fatigue tests performed. For the calculation of the amplitude stress, a fatigue stress concentration factor is used (Eq. (1))

$$K_f = 1 + q(K_t - 1) = 2.19 \tag{1}$$

where $K_t = 2.7$ is the stress concentration factor due to the presence of the hole, which is function of hole diameter and

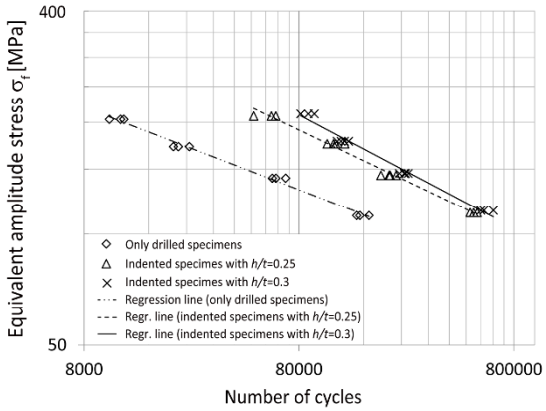

Fig. 16. Wöhler diagram for all the experimental tests.

plate width; q is the notch sensitivity, which can be calculated by the following Sines-Waisman equation (Eq. (2)).

$$q = \frac{1}{1 + \sqrt{\frac{b}{d/2}}} = 0.7 \tag{2}$$

where $b = 0.501$ for aluminum alloys and $d = 5.8$ mm is the hole diameter. However, since the mean stress value is different from zero, it is necessary to determine the equivalent amplitude stress σ_f, given by the Gerber line equation (Eq. (3)).

$$\sigma_f = \sigma_a \sqrt{\frac{1}{1 - \left(\frac{\sigma_m}{\sigma_u}\right)^2}} \tag{3}$$

where $\sigma_u = 310$ MPa is the ultimate stress of the AW 6082-T6 aluminum alloy; σ_a and σ_m are, respectively, the alternating stress amplitude and the mean tensile stress. From Fig. 16 it can be observe that the indentation process, performed before the drilling phase, significantly increases the fatigue life of the drilled plate. In fact, for a given value of cycles to failure, specimens subjected to indentation process show an increment of equivalent amplitude stress of about 45%, compared to the only drilled specimens. For high values of equivalent amplitude stress, the comparison between responses of type B and C specimens shows that the latter one reaches the failure condition for a number of cycles greater than 35%. For low values of equivalent amplitude stress, the relative difference between the two specimen types (B and C) decreases to 12%.

7. Conclusions

The present paper proposes a numerical and experimental study on aluminum alloy specimens subjected to an indentation process before that the drilling phase is performed.

The aim of the work is to study, by means of finite element

analysis, the contribution of the process parameters on the static and dynamic performance of drilled structural components. In order to identify optimal solutions, several numerical analysis are conducted. In particular, numerical analysis are focused on the evaluation of the compressive circumferential stress for different indenter radius and indentation depth.

The study shows that the indentation technique can lead to significant improvements to fatigue life on drilled plates. Optimal solution is obtained for an indentation depth corresponding to the 60% of the thickness of the plate and a final diameter of the hole equal to d = 5.8 mm, corresponding to the value of the diameter of spherical cavity induced on the specimen.

In the work, several experimental tests are conducted in order to evaluate the effects of indentation process on fatigue life. In detail, results for only drilled specimens and specimens subjected to indentation process (with different indentation depth) are compared. For the latter ones, a significant improvement on the fatigue life is observed.

In conclusion, the study shows that the procedure induces a significant delay on crack propagation and, consequently, in the fatigue fracture. Its use is therefore recommended for demanding applications, especially in the aeronautical field.

Nomenclature

d	: Hole diameter
r	: Radial distance from the hole axis
z	: Out-of-plane displacement
h	: Indentation depth
t	: Specimen thickness
D_e	: Outer diameter in the numerical model
a	: Radius of the spherical cavity
K_f	: Fatigue stress concentration factor
K_t	: Static stress concentration factor
q	: Notch sensitivity
σ_u	: Ultimate stress of the aluminum alloy

References

[1] S. Yoon, J. Park and N. Choi, Fatigue life analysis of shot-peened bearing steel, *Journal of Mechanical Science and Technology*, 26 (6) (2012) 1747-1752.

[2] J. Im, R. V. Grandhi and Y. Ro, Residual stress behaviors induced by laser peening along the edge of curved models, *Journal of Mechanical Science and Technology*, 26 (12) (2012) 3943-3952.

[3] G. Marannano, G. V. Mariotti, L. D'Acquisto, G. Restivo and N. Gianaris, Effect of cold working and ring indentation on fatigue life of aluminum alloy specimens, *Experimental Techniques*, 39 (3) (2015) 19-27.

[4] Y. C. Hsu and R. G. Forman, Elastic-plastic analysis of an infinite sheet having a circular hole under pressure, *J. Appl. Mech.*, 42 (2) (1975) 347-352.

[5] D. L. Rich and L. F. Impellizzeri, Fatigue analysis of cold-worked and interference fit fastener holes, *ASTM Spec. Tech. Publ.*, 637 (1977) 153-175.

[6] L. D'Acquisto and S. Pasta, On the measurement and Prediction of the Out-of-Plane Displacement Surrounding Cold-Expanded Holes, *Experimental Mechanics*, 51 (2011) 11-22.

[7] M. O. Lai and Z. He, Residual stress field of ballised holes, *Journal of Mechanical Science and Technology*, 26 (5) (2012) 1555-1565.

[8] C. G. C. Poussard, M. J. Pavier and D. J. Smith, Prediction of residual stresses in cold worked fastener holes using finite element method, *ASME PD64-8*, 1A (1994) 47-53.

[9] T. N. Chakherlou, Y. Alvandi and A. Kiani-Tabrizi, On the fatigue behavior of cold expanded fastener holes subjected to bolt tightening, *Int. J. Fatigue*, 33 (2011) 800-810.

[10] S. Ismonov, S. R. Daniewicz, J. C. Newman, M. R. Hill and M. R. Urban, Three dimensional finite element analysis of a split-sleeve cold expansion process, *Journal of Engineering Materials and Technology*, 131 (3) (2009).

[11] A. Aid, Z. Semari and M. Benguediab, Cold expansion effect on the fatigue crack growth of Al 6082: Numerical investigation, *Structural Engineering and Mechanics*, 49 (2) (2014) 225-235.

[12] R. Seifi, M. H. Zolfaghari and A. Shirazi, Experimental and numerical study of residual stresses caused by cold expansion of adjacent holes, *Meccanica*, 49 (2014) 687-706.

[13] C. Kim, D. J. Kim, C. S. Seok and W. H. Yang, Finite element analysis of the residual stress by cold expansion method under the influence of adjacent holes, *J. Mater. Process Technol.*, 153-154 (2004) 986-991.

[14] T. N Chakherlou, Y. Alvandi and A. Kiani-Tabrizi, On the fatigue behavior of cold expanded fastener holes subjected to bolt tightening, *Int. J. Fatigue*, 33 (6) (2011) 800-810.

[15] P. S. Baburamani, R. Ogden, Q. Liu and P. K. Sharp, Fatigue of cold expanded open hole coupons with pre-existing cracks, *Advanced Materials Research*, 891-892 (2014) 69-74.

[16] E. T. Easterbrook and M. A. Landy, *Evaluation of stress wave cold working (SWCW) process on high-strength aluminum alloys for aerospace*, StressWave Inc. (2009).

[17] *Technical report AL-02 fatigue testing of 2024 low load transfer aluminum specimens*, Stress Wave^{TM} (2001).

[18] *Technical report AL-06 fatigue testing of 0.040 inch thick 2024-T3 aluminum*, Stress Wave^{TM} (2001).

[19] J. Jang, Estimation of residual stress by instrumented indentation: A review, *Journal of Ceramic Processing Research*, 10 (3) (2009) 391-400.

[20] G. Feng, S. Qu, Y. Huang and W. D. Nix, An analytic expression for the stress field around an elastoplastic indentation/contact, *Acta Materialia*, 55 (2007) 2929-2938.

[21] G. Feng, S. Qu, Y. Huang and W. D. Nix, An quantitative analysis for the stress field around an elastoplastic indentation/contact, *Journal of Materials Research*, 42 (2009) 704-718.

[22] F. Yang, L. Peng and K. Okazaki, Effect of the indenter size on the indentation of aluminum, *Materials Characterization*, 57 (2006) 321-332.

[23] E. H. Yoffe, Elastic stress-fields caused by indenting brittle materials, *Philosophical Magazine A*, 46 (1982) 617-628.

[24] S. S. Chiang, D. B. Marshall and A. G. Evans, The response of solids to elastic plastic indentation, Stresses and residual-stresses, *Journal of Applied Physics*, 53 (1982) 298-311.
[25] B. Noble and D. A. Spence, *Formulation of two-dimensional and axisymmetric problems for an elastic half-space*, Mathematics Research Center, University of Wisconsin, Madison WI, USA (1971).
[26] R. Hill, *The mathematical theory of plasticity*, Clarendon Press, UK (1983).
[27] R. D. Mindlin and D. H. Cheng, Thermoelastic stress in semi-infinite solid., *J. Appl. Phys.*, 21 (1950) 931-933.
[28] R. L. Jackson and I. Green, A finite element study of elasto-plastic hemispherical contact against a rigid flat, *J. Tribol.*, 127 (2) (2005) 343-354.
[29] B. Taljat and G. M Pharr, Development of pile-up during spherical indentation of elastic-plastic solids, *Int. J. Solids Struct.*, 41 (2004) 3891-3904.

Giuseppe Marannano is a researcher at the University of Palermo and Assistant Professor of machine design. His main research areas are mechanics of composite materials, numerical methods, experimental stress analysis, fatigue fracture and material design.

Antonio Pasta is a full professor at the University of Palermo (Italy). His research interests are fatigue fracture and material design, fatigue behavior of materials and composites, experimental methods for composites.

Francesco Parrinello is a researcher at the University of Palermo and Professor of Computational Mechanic of Structures. His main research areas are non-local damage and constitutive models, interface constitutive modelling, kinematical modelling of strong discontinuity by extended finite element method.

Antonio Giallanza is a researcher at the University of Palermo and Assistant Professor of mechanical plants and project management. His main research areas are analysis and design of industrial plants and general services of plant.